

Analytical Solutions of the Displacement and Stress Fields of the Nanocomposite Structure of Biological Materials

Gang Liu^{1,3}, Baohua Ji^{1,2†}, Keh-Chih Hwang^{1†}, Boo Cheong Khoo^{3†}

¹ AML, Department of Engineering Mechanics, Tsinghua University, Beijing 100084, China

² Biomechanics and Biomaterials Laboratory, Department of Applied Mechanics, Beijing Institute of
Technology, Beijing 100081, China

³ Singapore -MIT Alliance, Department of Mechanical Engineering, National University of Singapore,
Kent Ridge, Singapore 119260, Singapore

Short title: Stress in the nanocomposite structure

Key Words: Biological materials; Nanocomposite structure; TSC model; Stress analysis; Perturbation
method

[†] Corresponding authors: Email: bhji@bit.edu.cn (BJ); mpekbk@nus.edu.sg (BCK); huangkz@mail.tsinghua.edu.cn (KCH)

Abstract: Biological materials such as bone, teeth and nacre are nanocomposites of protein and mineral with superior mechanical properties. The basic building blocks of these materials feature a generic nanocomposite structure with staggered alignment of mineral platelets in protein matrix. Because of the structural complexity of the generic structure, its displacement and stress fields are currently still unknown. In this study, a perturbation method was applied for analytically solving the displacement and stress fields of the generic nanocomposite structure. The effect of the elastic modulus, aspect ratio and volume fraction of mineral and protein on the displacement and stress fields in the nanocomposite structure was studied. A non-dimensional parameter γ was then suggested for characterizing the stress and strain fields in this nanostructure. We showed that the assumption of uniform shear stress distribution at the mineral-protein interface in the TSC model is valid when γ is less than 4 which is broadly applicable to most biological materials. The analytical solutions of displacement and stress fields obtained in this study provide a solid basis for further analyses of mechanical properties, such as the buckling and the fracture behaviors, etc., of biological materials.

1. Introduction

Biological hard tissues such as bone, teeth and shells, have superior mechanical properties through complex microstructure designs. These materials are normally organic-inorganic composites consisting of hard mineral crystals and soft protein matrix at different length scales [1-6]. The most elementary structures of these biological materials exhibit a convergent, exquisite ultrastructure at the nanoscale consisting of plate-like mineral crystals with large aspect ratio embedded in a soft collagen matrix, as shown schematically in Figure 1. In the past ten years, intensive efforts [7] have been made to address the mechanisms of high strength and toughness of the biological materials from various points of view including their hierarchical structures [1-3], reduction of stress concentration at crack tip [8], and protein-mineral interface roughness [9]. However, increasing evidence suggested that the generic nanocomposite structure was also crucial to the superior strength and toughness of biological materials [10]. Based on the studies of Jager and Fratzl [11] on the staggered arrangement of bone fibrils, Gao and coworkers developed the so-called tension-shear chain model (TSC) [12] to describe the mechanics of the generic nanostructure [13-15]. Subsequently, the TSC model was further applied to study other mechanical properties of biological materials, for instance, the structural stability of the nanocomposite structure and the interface strength between the protein and mineral, etc [16-18].

Although the TSC model has been successfully applied to studying different mechanical properties of biological materials at different length scales [7, 19], the assumptions and simplifications made during the development of the model have not been proved. For example, it assumes that the distribution of shear stress in protein as well as mineral-protein interface is uniform. Because of the structural complexity of the nanocomposite structure, the verification of this assumption is apparently not straightforward. The shear-lag model [20-22] has been applied for analyzing the displacement and stress in the nanocomposite

structure, obtaining approximate shear stress at protein-mineral interface and average normal stress in mineral. These studies to some extent provided support for the TSC model. However, the shear-lag model is only an approximate model for the nanocomposite structure, of which the assumptions and predictions still need rigorous validation. Moreover, the shear-lag model can only provide one dimensional distribution of the displacement and stress in the nanostructure.

This study is aimed to analyze the distribution of displacement and stress in the nanostructure and how these fields change with the aspect ratio of mineral crystal and the elastic modulus ratio of mineral to protein. A perturbation method will be applied to solve for the displacement and stress fields in the generic nanocomposite structure by treating the mechanical model as a plane stress problem.

2. Model

Figure 1(a) is the schematic illustration of a representative volume of the nanocomposite structure of biological materials, showing a large aspect ratio of mineral crystals and a staggered alignment of the mineral crystals in the protein matrix. According to the symmetry of the nanostructure, a unit cell extracted from Fig. 1(a) was adopted in this study for simplifying the analysis, as shown in Fig. 1(b), where the two mineral crystals are denoted as mineral *I* and mineral *II*, respectively. l is the length of mineral, d_m is the thickness of mineral, d_p is the thickness of protein, and h is thickness of protein at the mineral tip along the longitudinal direction. The subscripts m and p stand for the mineral and protein, respectively. Because h is much smaller than l , and protein is much softer than mineral, we further assume $h \sim 0$, and then Fig. 1 (b) is simplified to Fig. 2.

3. Perturbation Method

3.1 Basic Equations

According to the classical theory of elasticity, the equilibrium equation of the system in the absence of body forces is given as

$$\sigma_{ij,j} = 0 \quad (1)$$

and the isotropic constitutive relation is

$$\varepsilon_{ij} = \frac{1+\nu}{E} \sigma_{ij} - \frac{\nu}{E} \sigma_{kk} \delta_{ij} \quad (2)$$

where E and ν are the Young's modulus and the Poisson's ratio, respectively, and σ_{ij} and ε_{ij} are the stress tensor and strain tensor, respectively. For small deformation condition, the strain tensor is related to the displacement vector u_i by

$$\varepsilon_{ij} = \frac{1}{2} (u_{i,j} + u_{j,i}) \quad (3)$$

For a plane-stress problem $i, j = (x, y)$, the equilibrium equations and the Hooke's law, respectively, reduce to

$$\frac{\partial \sigma_{xy}}{\partial y} + \frac{\partial \sigma_{xx}}{\partial x} = 0, \quad \frac{\partial \sigma_{xy}}{\partial x} + \frac{\partial \sigma_{yy}}{\partial y} = 0 \quad (4)$$

and

$$\varepsilon_{xx} = \frac{1}{E} (\sigma_{xx} - \nu \sigma_{yy}), \quad \varepsilon_{yy} = \frac{1}{E} (\sigma_{yy} - \nu \sigma_{xx}), \quad \varepsilon_{xy} = \frac{\sigma_{xy}}{2G}. \quad (5)$$

where G is the shear modulus. The strain is related to the displacements by

$$\varepsilon_{xx} = \frac{\partial u}{\partial x}, \quad \varepsilon_{yy} = \frac{\partial v}{\partial y}, \quad \varepsilon_{xy} = \frac{1}{2} \left(\frac{\partial u}{\partial y} + \frac{\partial v}{\partial x} \right). \quad (6)$$

where u and v are the displacement in x and y directions, respectively.

3.2 Perturbation expansion

For the convenience of analysis, we make coordinate transformation as $\xi = x/l$, $\eta = y/d_m$. Then we have $\partial/\partial x = \frac{1}{l}\partial/\partial \xi$, $\partial/\partial y = \frac{1}{d_m}\partial/\partial \eta$, $\partial^2/\partial x^2 = \frac{1}{l^2}\partial^2/\partial \xi^2$, and $\partial^2/\partial y^2 = \frac{1}{d_m^2}\partial^2/\partial \eta^2$. The origin and directions of the new coordinates (ξ, η) are consistent with the original (x, y) coordinates, as shown in Fig. 2. Furthermore, we set

$$C_E = E_p \epsilon_d^{-2} / E_m, \quad C_G = G_p \epsilon_d^{-2} / G_m \quad (7)$$

where $\epsilon_d = d_m/l$, then we have

$$1/E_p = \epsilon_d^{-2} / (E_m C_E), \quad 1/G_p = \epsilon_d^{-2} / (G_m C_G), \quad C_E = (1 + \nu_p) C_G / (1 + \nu_m). \quad (8)$$

Note that $\rho = l/d_m = \epsilon_d^{-1}$ is the aspect ratio of the mineral. For the biological materials, such as bone and dentin, $E_p/E_m \sim 1/1000$ and $\epsilon_d = d_m/l \sim 1/30$, therefore we have $C_E \sim C_G \sim O(1)$. ϵ_d is a small parameter in this work.

In the new coordinate system (ξ, η) , the equilibrium equation Eq. (4) and geometric equation Eq. (6) can be transformed, respectively, as

$$\epsilon_d^{-1} \frac{\partial \sigma_{xy}}{\partial \eta} + \frac{\partial \sigma_{xx}}{\partial \xi} = 0, \quad \frac{\partial \sigma_{xy}}{\partial \xi} + \epsilon_d^{-1} \frac{\partial \sigma_{yy}}{\partial \eta} = 0 \quad (9)$$

and

$$\varepsilon_{xx} = \frac{1}{l} \frac{\partial u}{\partial \xi}, \quad \varepsilon_{yy} = \frac{\epsilon_d^{-1}}{l} \frac{\partial v}{\partial \eta}, \quad \varepsilon_{xy} = \frac{1}{2l} \left(\epsilon_d^{-1} \frac{\partial u}{\partial \eta} + \frac{\partial v}{\partial \xi} \right). \quad (10)$$

It is not possible to directly solve the governing equations, Eqs. (5), (9) and (10), due to the structural complexity of the model depicted in Fig. 2. Here, we adopt the perturbation method to simplify the analyses. We first analyse the order of magnitude of the stress in mineral and protein. Considering the elastic modulus of the mineral is order of magnitude ϵ_d^{-2} higher than that of protein, as well as the loading transfer relation between protein and mineral in the nano-composite structure, we assume that

$\epsilon_d^2 \sigma_{xx}^m \sim \sigma_{xx}^p$, $\sigma_{xy}^m \sim \sigma_{xy}^p$, $\sigma_{yy}^m \sim \sigma_{yy}^p$. Therefore, we have that the stress distribution in the mineral crystals as $\epsilon_d^2 \sigma_{xx}^m \sim \epsilon_d \sigma_{xy}^m \sim \sigma_{yy}^m$ by considering the large aspect ratio of mineral, and the stress distribution in protein layer as $\sigma_{xx}^p \sim \epsilon_d \sigma_{xy}^p \sim \sigma_{yy}^p$.

Subsequently, the expansions of the strain components can be obtained according to the expansion of stress components and the constitutive relations. The expansions of the displacement can be obtained by considering the large aspect ratio of mineral crystal, the expansions of the strain components and the constitutive relations. Based on the above assumption, we proposed a perturbation expansion method for the stress, strain and displacement expressions. For the mineral crystals, the expansions are

$$\begin{cases} \sigma_{xx}^m = \sigma_{xx}^{m(0)} + \epsilon_d^2 \sigma_{xx}^{m(1)} + \dots, \\ \sigma_{yy}^m = \epsilon_d^2 (\sigma_{yy}^{m(0)} + \epsilon_d^2 \sigma_{yy}^{m(1)} + \dots), \\ \sigma_{xy}^m = \epsilon_d (\sigma_{xy}^{m(0)} + \epsilon_d^2 \sigma_{xy}^{m(1)} + \dots), \end{cases} \quad (11)$$

$$\begin{cases} \epsilon_{xx}^m = \epsilon_{xx}^{m(0)} + \epsilon_d^2 \epsilon_{xx}^{m(1)} + \dots, \\ \epsilon_{yy}^m = \epsilon_{yy}^{m(0)} + \epsilon_d^2 \epsilon_{yy}^{m(1)} + \dots, \\ \epsilon_{xy}^m = \epsilon_d (\epsilon_{xy}^{m(0)} + \epsilon_d^2 \epsilon_{xy}^{m(1)} + \dots), \end{cases} \quad (12)$$

$$\begin{cases} u^m = u^{m(0)} + \epsilon_d^2 u^{m(1)} + \dots, \\ v^m = \epsilon_d (v^{m(0)} + \epsilon_d^2 v^{m(1)} + \dots), \end{cases} \quad (13)$$

and for the protein layers are

$$\begin{cases} \sigma_{xx}^p = \epsilon_d^2 (\sigma_{xx}^{p(0)} + \epsilon_d^2 \sigma_{xx}^{p(1)} + \dots), \\ \sigma_{yy}^p = \epsilon_d^2 (\sigma_{yy}^{p(0)} + \epsilon_d^2 \sigma_{yy}^{p(1)} + \dots), \\ \sigma_{xy}^p = \epsilon_d (\sigma_{xy}^{p(0)} + \epsilon_d^2 \sigma_{xy}^{p(1)} + \dots), \end{cases} \quad (14)$$

$$\begin{cases} \varepsilon_{xx}^p = \varepsilon_{xx}^{p(0)} + \varepsilon_d^2 \varepsilon_{xx}^{p(1)} + \dots, \\ \varepsilon_{yy}^p = \varepsilon_{yy}^{p(0)} + \varepsilon_d^2 \varepsilon_{yy}^{p(1)} + \dots, \\ \varepsilon_{xy}^p = \varepsilon_d^{-1} \left(\varepsilon_{xy}^{p(0)} + \varepsilon_d^2 \varepsilon_{xy}^{p(1)} + \dots \right), \end{cases} \quad (15)$$

$$\begin{cases} u^p = u^{p(0)} + \varepsilon_d^2 u^{p(1)} + \dots, \\ v^p = \varepsilon_d \left(v^{p(0)} + \varepsilon_d^2 v^{p(1)} + \dots \right), \end{cases} \quad (16)$$

Substituting the expansions Eq. (11) and (12) into Eq. (5) and (9), and Eq. (12) and (13) into Eq.(10), we obtain the expansions of the constitutive relations, equilibrium equations and the geometric equations of mineral. Similarly, substituting the expansions Eq. (14) and (15) into Eq. (5) and (9), and Eq. (15) and (16) into Eq.(10), we obtain the expansions of the corresponding governing equations of protein.

3.3 Boundary conditions

We apply the symmetric boundary conditions at the top surface of mineral *I* (line *AB*) and the bottom surface of mineral *II* (line *GH*). The traction free boundary conditions are applied at the left end of the mineral *I* (line *AC*) and the right end of the mineral *II* (line *FH*). (The tensile force by protein at the mineral tip is negligible because it is much weaker than that in mineral) The unit displacement loading $u_0/2 = \pm 1$ was applied on the right end of the mineral *I* (line *BD*) and the left end of the mineral *II* (line *EG*), respectively, as shown in Fig. 2. According to the perturbation expansion of displacement given in Eq.(13), we have

$$u_0/2 = u_0^{(0)}/2 + \varepsilon_d^2 u_0^{(1)}/2 = \pm 1 \quad (17)$$

and

$$u_0^{(0)}/2 = \pm 1, \text{ and } u_0^{(1)}/2 = 0. \quad (18)$$

4. Analytical Solutions

According to the perturbation expansion given in section 3.2, the perturbation solution of the governing equations of each expansion term can be solved successively. Firstly, we will solve the first expansion term of the governing equations (the initial solution). The corresponding governing equations for the first expansion term of the mineral layer are given as following

$$\begin{cases} \varepsilon_{xx}^{m(0)} = \frac{1}{E_m} \sigma_{xx}^{m(0)} = \frac{1}{l} \frac{\partial u^{m(0)}}{\partial \xi} \\ \varepsilon_{yy}^{m(0)} = -\frac{\nu_m}{E_m} \sigma_{xx}^{m(0)} = \frac{1}{l} \frac{\partial v^{m(0)}}{\partial \eta} \\ \varepsilon_{xy}^{m(0)} = \frac{1}{2G_m} \sigma_{xy}^{m(0)} \end{cases} \quad (19)$$

and

$$\frac{\partial u^{m(0)}}{\partial \eta} = 0 \quad (20)$$

and

$$\begin{cases} \frac{\partial \sigma_{xy}^{m(0)}}{\partial \eta} + \frac{\partial \sigma_{xx}^{m(0)}}{\partial \xi} = 0 \\ \frac{\partial \sigma_{xy}^{m(0)}}{\partial \xi} + \frac{\partial \sigma_{yy}^{m(0)}}{\partial \eta} = 0. \end{cases} \quad (21)$$

Solving Eqs. (19), (20) and (21), we can obtain the analytical initial solution of the displacement and stress components as below,

$$\left\{ \begin{array}{l} u_i^{m(0)} = f_i^{(0)}(\xi) \\ v_i^{m(0)} = -\nu_m \eta f_i^{(0)'}(\xi) + g_i^{(0)}(\xi) \\ \sigma_{xx,i}^{m(0)} = \frac{E_m}{l} f_i^{(0)'}(\xi) \\ \sigma_{xy,i}^{m(0)} = -\frac{E_m}{l} \eta f_i^{(0)''}(\xi) + \lambda_i^{(0)}(\xi) \\ \sigma_{yy,i}^{m(0)} = \frac{E_m}{2l} \eta^2 f_i^{(0)'''}(\xi) - \eta \lambda_i^{(0)'}(\xi) + \chi_i^{(0)}(\xi) \end{array} \right. \quad (22)$$

where the subscript $i=I$ and II , standing for mineral I and mineral II , respectively. The unknown functions of $f_i^{(0)}(\xi)$, $g_i^{(0)}(\xi)$, $\lambda_i^{(0)}(\xi)$, $\chi_i^{(0)}(\xi)$ can be obtained by applying the symmetric conditions at lines AB and GH and the continuity condition at the protein-mineral interface. The detailed procedures can be found in Appendix A of the Electronic Supplementary Materials (ESM).

Next, we carried out the analysis for the protein layer with the same procedures. The corresponding governing equations for the initial solution of the protein are

$$\left\{ \begin{array}{l} \varepsilon_{xx}^{p(0)} = \frac{1}{E_m C_E} (\sigma_{xx}^{p(0)} - \nu_p \sigma_{yy}^{p(0)}) = \frac{1}{l} \frac{\partial u^{p(0)}}{\partial \xi} \\ \varepsilon_{yy}^{p(0)} = \frac{1}{E_m C_E} (\sigma_{yy}^{p(0)} - \nu_p \sigma_{xx}^{p(0)}) = \frac{1}{l} \frac{\partial v^{p(0)}}{\partial \eta}, \\ \varepsilon_{xy}^{p(0)} = \frac{1}{2G_m C_G} \sigma_{xy}^{p(0)} = \frac{1}{2l} \frac{\partial u^{p(0)}}{\partial \eta} \end{array} \right. \quad (23)$$

and

$$\left\{ \begin{array}{l} \frac{\partial \sigma_{xy}^{p(0)}}{\partial \eta} = 0 \\ \frac{\partial \sigma_{xy}^{p(0)}}{\partial \xi} + \frac{\partial \sigma_{yy}^{p(0)}}{\partial \eta} = 0. \end{array} \right. \quad (24)$$

Solving Eqs.(23) and (24), we can obtain the initial solution for the protein as below

$$\left\{ \begin{array}{l} u^{p(0)} = \frac{l}{G_m C_G} \eta \kappa^{(0)}(\xi) + p^{(0)}(\xi) \\ v^{p(0)} = \frac{-l(1+\nu_p)^2}{2E_m C_E} \eta^2 \kappa^{(0)'}(\xi) + \frac{l(1-\nu_p^2)}{E_m C_E} \eta s^{(0)}(\xi) - \nu_p \eta p^{(0)'}(\xi) + q^{(0)}(\xi) \\ \sigma_{xx}^{p(0)} = (2+\nu_p) \eta \kappa^{(0)'}(\xi) + \frac{E_m C_E}{l} p^{(0)'}(\xi) + \nu_p s^{(0)}(\xi) \\ \sigma_{xy}^{p(0)} = \kappa^{(0)}(\xi) \\ \sigma_{yy}^{p(0)} = -\eta \kappa^{(0)'}(\xi) + s^{(0)}(\xi) \end{array} \right. \quad (25)$$

where the functions $\kappa^{(0)}(\xi)$, $p^{(0)}(\xi)$, $q^{(0)}(\xi)$, and $s^{(0)}(\xi)$ are obtained by applying the symmetric condition and the continuity condition at the protein-mineral interface. Again, details are provided in Appendix A of the Electronic Supplementary Materials (ESM).

Finally, substituting the displacement loading boundary condition, $u_0^{(0)}/2 = \pm 1$, we obtained the initial solution of the stress and displacement fields of mineral (the mineral *I* and mineral *II*) as,

$$u_i^{m(0)} = A \cdot \left(2\gamma \xi \operatorname{sh} \frac{\gamma}{4} \pm 2 \operatorname{ch} \gamma \xi \right) \quad (26)$$

$$v_i^{m(0)} = A \cdot \left(2\gamma \nu_m \left(\frac{d_m + d_p}{2d_m} \mp \eta \right) \left(\operatorname{sh} \gamma \xi \pm \operatorname{sh} \frac{\gamma}{4} \right) \mp \frac{(\nu_m d_m + \nu_p d_p) \gamma \operatorname{sh} \frac{\gamma}{4}}{d_m} \right) \quad (27)$$

$$\sigma_{xx,i}^{m(0)} = A \frac{E_m}{l} \left(2\gamma \operatorname{sh} \frac{\gamma}{4} \pm 2\gamma \operatorname{sh} \gamma \xi \right) \quad (28)$$

$$\sigma_{yy,i}^{m(0)} = A \frac{E_m}{l} \left(\pm \eta^2 - \frac{(d_m + d_p)}{d_m} \eta \pm \frac{d_p^2}{4d_m^2} \right) \gamma^3 \operatorname{sh} \gamma \xi \quad (29)$$

$$\sigma_{xy,i}^{m(0)} = A \frac{E_m}{l} \frac{(d_m + d_p \mp 2\eta d_m)}{d_m} \gamma^2 \operatorname{ch} \gamma \xi \quad (30)$$

where $A = u_0^{(0)} / \left(\gamma \operatorname{sh} \frac{\gamma}{4} + 4 \operatorname{ch} \frac{\gamma}{4} \right)$, $\operatorname{ch} \gamma \xi = (e^{\gamma \xi} + e^{-\gamma \xi})/2$, $\operatorname{sh} \gamma \xi = (e^{\gamma \xi} - e^{-\gamma \xi})/2$,

$G_m = E_m / (2(1+\nu_m))$, and

$$\gamma = 2\rho \sqrt{\frac{G_p d_m}{E_m d_p}} = 2\rho \sqrt{\frac{G_p \Phi}{E_m (1-\Phi)}} \quad (31)$$

where $\Phi = d_m/(d_m + d_p)$ is the volume fraction of mineral in the nanocomposite structure.

Similarly, we obtain the initial solution of the protein layer as

$$u^{p(0)} = A \cdot \left(2\gamma \xi \operatorname{sh} \frac{\gamma}{4} + \frac{4d_m \eta \operatorname{ch} \gamma \xi}{d_p} \right) \quad (32)$$

$$v^{p(0)} = A \cdot \left(\left(-\frac{(1+\nu_p)d_m}{d_p} \eta^2 + \frac{(1+\nu_p)d_p}{4d_m} + \nu_m \right) \gamma \operatorname{sh} \gamma \xi - 2\eta \nu_p \gamma \operatorname{sh} \frac{\gamma}{4} \right) \quad (33)$$

$$\sigma_{xx}^{p(0)} = A \frac{E_m}{l} \left((2+\nu_p) \eta \gamma^3 \operatorname{sh} \gamma \xi + \frac{(1+\nu_p)d_p}{d_m} \gamma^3 \operatorname{sh} \frac{\gamma}{4} \right) \quad (34)$$

$$\sigma_{yy}^{p(0)} = -A \frac{E_m}{l} \eta \gamma^3 \operatorname{sh} \gamma \xi \quad (35)$$

$$\sigma_{xy}^{p(0)} = A \frac{E_m}{l} \gamma^2 \operatorname{ch} \gamma \xi. \quad (36)$$

Substituting Eqs. (26)-(30) into Eq. (11) and (13), and Eqs. (32)-(36) into Eq. (14) and (16), we obtain the approximate perturbation solution based on the initial solution. To improve the precision of the solution, we should solve the higher order terms of perturbation corrections. To give an example, the first order perturbation correction was solved in Appendix B of the Electronic Supplementary Materials (ESM). The other higher order perturbation corrections can be solved systematically in the same spirit.

5. Results and Discussions

To check the convergence of the perturbation solutions, we make comparison of the displacement and stress fields between the initial solution (Eqs.(26) to (36)) and the combination of the initial solution and the first order perturbation correction (Eqs.(B82) to (B91) in the ESM). Figure 3 shows the comparison of the normal stress, shear stress and longitudinal displacement in mineral I at $\eta = d_p/(2d_m)$ (i.e. at the mineral-protein interface) for different aspect ratios. It is clear that, the results of the initial solution are

very close to those of the combination of the initial solution and the first order perturbation. Therefore, the initial solution can appropriately describe the stress and displacement fields in the nanocomposite structure under tension or compression. In the following analyses, we will only adopt the approximate perturbation solutions from the initial solutions (Eqs. (26) to (36)).

To further check the validity of our analytical solutions, we made comparison with the FEM calculations using ABAQUS software (Version 6.4-1). The FEM model corresponds to the mechanical model shown in Fig. 2. We applied symmetry boundary conditions on GH and kept AB as straight line in the FEM simulations. The structure was loaded in tension at BD and EG . Figures S1 (in ESM) shows the normal stress (Fig. S1a), the shear stress (Fig. S1b) and the axial displacement (Fig. S1c) in mineral I in the longitudinal direction at the interface $\eta = d_p / (2d_m)$. We can see that our theoretical predictions agree well with the FEM results except at the tips of mineral. We also note that the shear stress $l\sigma_{xy,I}^m / (u_0 E_m)$ along the interface is almost uniform, and the smaller the aspect ratio, the more uniform is its distribution. This result is consistent with the assumption made in the TSC model, explaining why the predictions of the TSC Model [12] agree with the experimental observations.

Based on Eq.(26) and Eq.(28), one can derive the equivalent Young's modulus \hat{E} of the biological nanocomposite structure as

$$\frac{1}{\hat{E}} = \frac{1}{E_m \Phi} + \frac{4}{E_m \Phi \gamma \tanh(\gamma/4)} \quad (37)$$

The prediction of Eq. (37) was compared with those of the TSC model and the FEM calculations as shown in Fig. 4 and Fig.S2. We can see that Eq. (37) agrees well with the TSC model at relative small aspect ratio of mineral crystal, but its prediction deviates from that of the TSC model at larger aspect ratio. In contrast, Eq. (37) is consistent with the FEM calculation at a much larger range of aspect ratio. It is

noted that when $\gamma/4$ is sufficiently small, we can approximate $\tanh(\gamma/4) \sim \gamma/4$, Eq. (37) will degenerate exactly to the Eq.(1) of the TSC model in reference [12].

With the theoretical solutions in Eqs. (26) to (36), we can study the influence of elastic modulus of mineral and protein on the stress and displacement distribution in the nanostructure. Figure S3 illustrates the normal stress (Fig. S3a), shear stress (Fig. S3b) and the displacement (Fig. S3c) along the longitudinal direction of the mineral at different E_m/G_p values. From Fig. S3 we can see that increasing the ratio of Young's modulus of mineral to shear modulus of protein will cause the decrease of the normalized normal stress in the mineral and the normalized shear stress at the mineral-protein interface. The mechanism is that with the increase of elastic modulus of mineral relative to protein's, the normalized equivalent Young's modulus of the nanocomposite structure will decrease, according to Eq.(37). Under the same displacement loading, the force acted on the nanocomposite structure will decrease, therefore the mineral will take less load in the nanocomposite structure and the interface transfer less shear stress. However, because the mineral becomes stiffer (or protein becomes softer), the deformation of mineral will be smaller. Moreover, the shear stress becomes more uniform with the increase of the elastic modulus of mineral crystals. It implies that the larger difference in elastic modulus between mineral and protein will induce more uniform shear stress at the mineral-protein interface.

According to Eq.(28) and Eq.(30), we find that the parameter $\gamma = 2\rho\sqrt{G_p\Phi/(E_m(1-\Phi))}$ (i.e. Eq.(31)) determines the nature of the distribution of shear stress at the mineral-protein interface and the normal stress in mineral. We calculated the dimensionless shear stress $l\sigma_{xy,I}^m/(u_0E_m)$ and normal stress $l\sigma_{xx,I}^m/(u_0E_m)$ as γ changes in the range from 2.0 to 20. Figure 5 and Fig. S4 show the distribution of these two stress components, respectively. We can see that the shear stress distribution is almost uniform

and the normal stress along the length of mineral crystals is almost linear when $\gamma \leq 4$. However, the distribution of the shear stress at the interface becomes non-uniform and the normal stress along the length of the mineral becomes nonlinear when $\gamma > 4$. As noted, γ is determined by the aspect ratio ρ , volume fraction Φ of mineral, Young's modulus ratio of mineral to protein E_m/E_p , and Poisson's ratio of protein ν_p . Therefore, the smaller the aspect ratio and the larger the modulus ratio, the smaller the value of γ . It is clear that the shear stress distribution along the interface is approximately uniform at an aspect ratio of approximately 30 and a Young's modulus ratio of approximately 1000, as in the case of real biological materials, which agrees with the basic assumption of the TSC model.

6. Conclusions

In this study, we adopted a more rigorous approach to analyze the stress and strain fields in the nanocomposite structure of biological materials on the basis of the 2D elasticity theory. Using a perturbation approach, we obtained the approximate analytical solution of not only the interfacial stress between protein and mineral but also the whole stress and strain fields in the nanocomposite structure given by Eqs. (26) to (36). We showed that the predictions of Eqs. (26) to (36) based only on the initial solutions are very close to those based on the combination of the initial solution and the first order perturbation (Eqs. (B82) to (B91) in the ESM). In comparison with previous studies, we for the first time obtained the analytical solutions of two dimensional distribution of the displacement and stress fields in the nanocomposite structure. This study may provide the basis for further analyses of other mechanical properties of biological materials, e.g. the buckling and failure behaviors, etc.

We showed that the smaller the aspect ratio and the larger the elastic modulus ratio of the nanostructure, the more uniform is the distribution of shear stress at the mineral-protein interface. This

feature can be described by the parameter γ which is defined by the aspect ratio, volume fraction of mineral, and the elastic modulus ratio of mineral to protein. When $\gamma \leq 4$, as in the case of real biological materials, the shear stress at the mineral-protein interface is almost uniform, which fully supports the basic assumption of the TSC model. However, one will not be able to assume a uniform distribution of shear stress at the interface and linear distribution of normal stress in the mineral along the longitudinal direction when $\gamma > 4$. This result can serve as a criterion whether the TSC model is applicable to a composite material with a similar microstructure as of the biological materials.

Acknowledgements:

GL gratefully acknowledges Prof. Yonggang Huang (Northwestern University, USA) for the fruitful discussions. BJ acknowledges the financial support from the National Natural Science Foundation of China through Grant No. 10732050, 10872115 and 11025208.

References:

- [1] Menig R, Meyers MH, Meyers MA, Vecchio KS. Quasi-static and dynamic mechanical response of *Haliotis rufescens* shells. *Acta Materialia* 2000;48:2383-2398.
- [2] Menig R, Meyers MH, Meyers MA, Vecchio KS. Quasi-static and dynamic mechanical response of *Strombus gigas*(conch) shells. *Materials Science & Engineering A*. 2001;297:203-211.
- [3] Kamat S, Su X, Ballarini R, Heuer AH. Structural basis for the fracture toughness of the shell of the conch *Strombus gigas*. *Nature*. 2000;405(6790):1036-1040.
- [4] Currey JD. Mechanical properties of mother of pearl in tension. *Proc R Soc London B*. 1977;196:443-463.
- [5] Jackson AP, Vincent JFV, Turner RM. The mechanical design of nacre. *Proc R Soc London B*. 1988;234:415-440.
- [6] Landis WJ. The Strength Of A Calcified Tissue Depends In Part On The Molecular-Structure And Organization Of Its Constituent Mineral Crystals In Their Organic Matrix. *Bone*. 1995;16(5):533-544.
- [7] Ji BH, Gao HJ. Mechanical Principles of Biological Nanocomposites. *Annual Review of Materials Research*. 2010;40:77-100.
- [8] Okumura K, de Gennes P-G. Why is nacre strong? Elastic theory and fracture mechanics for biocomposites with stratified structures. *The European Physical Journal E*. 2001;4:121-127.
- [9] Wang RZ, Suo Z, Evans AG, N. Y, Aksay IA. Deformation mechanisms in nacre. *Journal of Materials Research*.

2001;16:2485-2493.

- [10] Gao H, Ji B. Modeling fracture in nanomaterials via a virtual internal bond method. *Engineering Fracture Mechanics*. 2003;70(14):1777-1791.
- [11] Jager I, Fratzl P. Mineralized collagen fibrils: a mechanical model with a staggered arrangement of mineral particles. *Biophysical Journal*. 2000;79:1737-1746.
- [12] Gao HJ, Ji BH, Jaeger IL, Arzt E, Fratzl P. Materials become insensitive to flaws at nanoscale: Lessons from nature. *Proceedings of the National Academy Society of the United States of America*. 2003;100:5597-5600.
- [13] Ji B, Gao H. Mechanical properties of nanostructure of biological materials. *Journal of the Mechanics and Physics of Solids*. 2004;52(9):1963-1990.
- [14] Ji B, Gao H. A study of fracture mechanisms in biological nano-composites via the virtual internal bond model. *Materials Science and Engineering A-Structural Materials Properties Microstructure and Processing*. 2004;366(1):96-103.
- [15] Gao H, Ji B, Buehler MJ, Yao H. Flaw tolerant bulk and surface nanostructures of biological systems. *Mechanics and Chemistry of Biosystems*. 2004;1:37-52.
- [16] Ji BH, Gao HJ, Hsia KJ. How do slender mineral crystals resist buckling in biological materials? *Philosophical Magazine Letters*. 2004;84:631-641.
- [17] Ji BH. An Atomistic Study of the Strength of Protein-Mineral Interface of Biological Materials with a Biomimicking Model System at Nanoscale. *Journal of Computational and Theoretical Nanoscience*. 2010;7:1265-1271.
- [18] Ji BH. A study of the interface strength between protein and mineral in biological materials. *Journal of Biomechanics*. 2008;41:259-266.
- [19] Gao H. Application of fracture mechanics concepts to hierarchical biomechanics of bone and bone-like materials. *International Journal of Fracture*. 2006;138(1-4):101-137.
- [20] Kotha SP, Kotha S, Guzelsu N. A shear-lag model to account for interaction effects between inclusions in composites reinforced with rectangular platelets. *Composites Science and Technology*. 2000;60:2147-2158.
- [21] Zuo SC, Wei YG. Effective elastic modulus of bone-like hierarchical materials. *Acta Mechanica Solida Sinica*. 2007;20(3):198-205.
- [22] Chen B, Wu PD, Gao H. A characteristic length for stress transfer in the nanostructure of biological composites. *Composites Science and Technology*. 2009;69(7-8):1160-1164.

Figure captions

Figure 1: The generic nanocomposite structure of biological materials. (a) Schematic illustration of the staggered alignment of the mineral in the protein matrix; (b) a unit cell extracted from the nanocomposite structure according to the symmetry of the structure.

Figure 2: The simplified unit cell model for the analytical analysis. The structure is loaded at the right end of mineral *I* and the left end of mineral *II*.

Figure 3: The comparison between the predictions of the initial solution and the summation of the initial solution and the first order perturbation correction at three different aspect ratios of mineral. (a) The dimensionless normal stress in the mineral crystal; (b) the dimensionless shear stress along the mineral-protein interface; (c) the dimensionless displacement in the mineral along the longitudinal direction. $E_m/G_p = 2400$, and $\Phi = 50\%$.

Figure 4: The equivalent Young's modulus of the nanocomposite structure versus the aspect ratio of mineral crystal predicted by our analytical solution, the TSC model and the FEM simulation ($E_m/G_p = 2400$). The volume fraction of mineral $\Phi = 95\%$ (as the case of nacre)

Figure 5: The evolution of the distribution of the interface shear stress at the mineral-protein interface with the variation of the γ value.

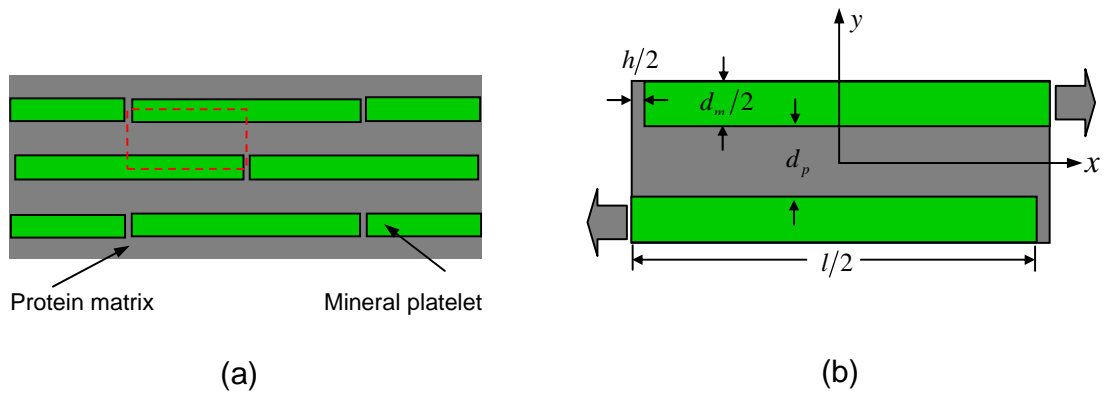


Figure 1

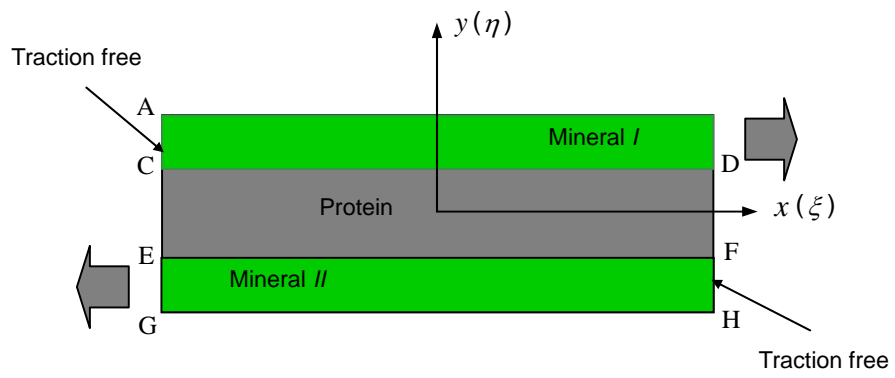


Figure 2

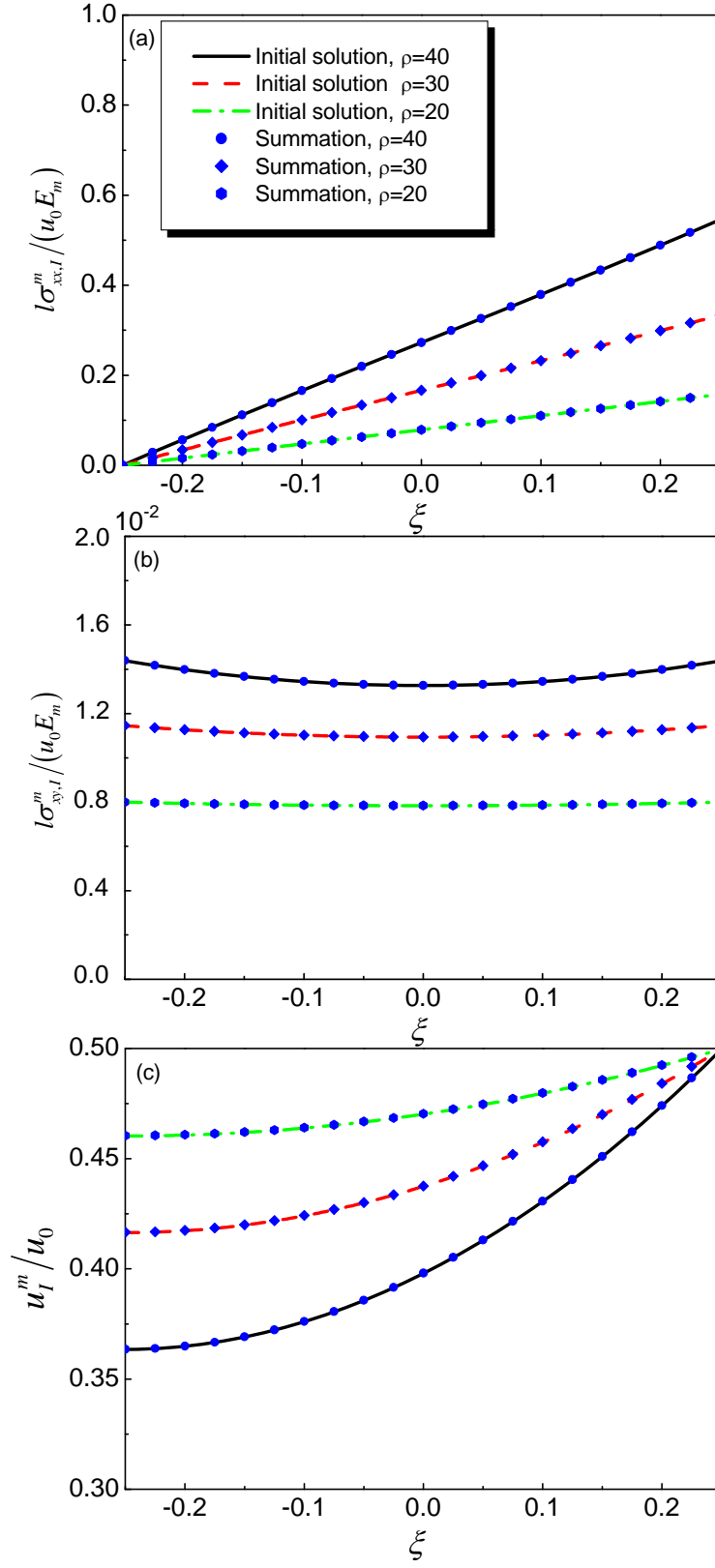


Figure 3

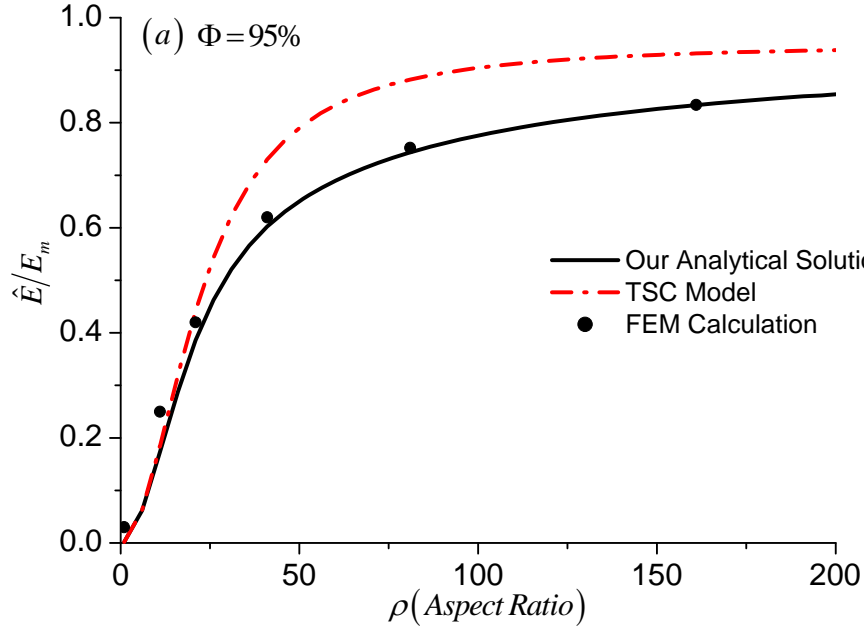


Figure 4

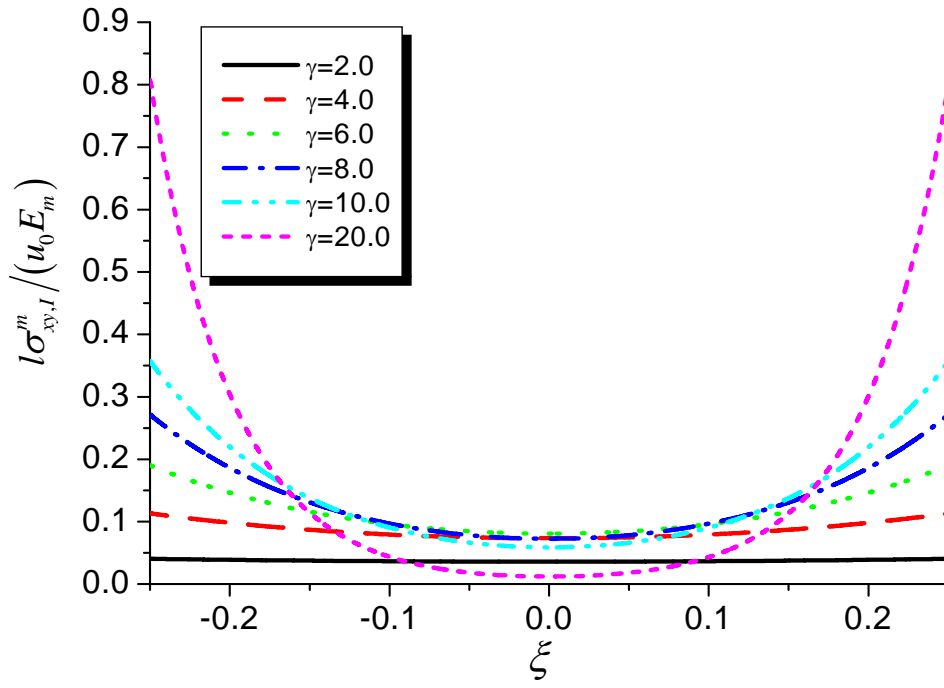


Figure 5